Vol. 24, No. 2(2025) Mat25443
Revista Mexicana de Ingeniería Química

Characterization and efficiency of *Luffa cylindrica* as bioadsorbent in Cr (VI) remotion from synthetic wastewater

Caracterización y eficiencia de *Luffa cilíndrica* como bioadsorbente en la remoción de Cr (VI) de aguas residuales sintéticas

J.G. Moreno-Rubio[1], N.R. Osornio-Rubio[1], H. Jiménez-Islas[2], E. Barrera-Calva[3] A.Y. Ramírez-Yañez[1], G.M. Martínez-González[1]*

[1]Departamento de Ingeniería Química, [2]Departamento de Ingeniería Bioquímica y Ambiental, Tecnológico Nacional de México en Celaya. Antonio García Cubas Pte. #600 esq. Av. Tecnológico. Celaya. Gto. México. C.P. 38010.

[3] Universidad Autónoma Metropolitana, Iztapalapa, Área de Ingeniería en Energía, IPH, CBI. Ciudad de México. México.

Received: October 17, 2024; Accepted: March 16, 2025

Abstract

This study investigated luffa as a bioadsorbent for removing Cr (VI) from synthetic wastewater. Luffa was characterized by scanning electron microscopy (SEM) and Fourier-transform infrared spectroscopy (FTIR), which mainly revealed a composition of carbon and oxygen, as identified via SEM. The morphology showed cylindrical fibers arranged in a network, with diameters ranging from 200 to 300 μm and surface fissures between 25 and 100 μm. FTIR analysis detected hydroxyl, carbonyl, and carboxyl functional groups responsible for adsorbing $HCrO_4^{-1}$. The composition of luffa was found to be 14% lignin, 76% cellulose, and 10% hemicellulose. Adsorption kinetics were evaluated at pH 2 using 0.5 g of luffa in 100 mL of synthetic wastewater, with Cr (VI) concentrations varying between 15 and 50 ppm. Sampling followed the NMX-AA-044-SCFI-2014 protocol, and Cr (VI) quantification was performed by UV-Vis spectrophotometry, achieving a removal efficiency of 100%. The adsorption kinetics were adjusted to a pseudo-second-order model using parameter estimation. Luffa demonstrated an adsorption capacity of 10.0 mg Cr (VI)/g, with energy-dispersive X-ray spectroscopy (EDS) revealing 1.21% Cr in dry luffa and 48.23% in calcined luffa, indicating Cr incorporation within the luffa structure. X-ray fluorescence (XRF) analysis detected 8.72% Cr in dry luffa and 75.07% in calcined luffa.

Keywords: Cr (VI), Luffa, Bioadsorption Kinetics, Wastewater.

Resumen

Se estudió la luffa como bioadsorbente para remover Cr (VI) de aguas residuales. La luffa se caracterizó mediante microscopia electrónica de barrido (SEM) y espectroscopia infrarroja (FTIR), encontrando con SEM, C y O principalmente. En la morfología se encontraron fibras cilíndricas en red con diámetros entre 200-300 μm y fisuras superficiales entre 25-100 μm. Con FTIR se encontraron grupos hidroxilo, carbonilo y carboxilo que adsorben $HCrO_4^{-1}$. La composición de la luffa fue 14 % lignina, 76% celulosa y 10% hemicelulosa. También, se determinó la cinética de adsorción a pH 2, con 0.5 gr de luffa en 100 mL de agua residual, empleando concentraciones de 15-50 ppm de Cr (VI). Se muestreó con NMX-AA-044-SCFI-2014 y se determinó el Cr (VI) por Espectrofotometría UV-Vis, obteniéndose una remoción del 100%. La cinética de adsorción se ajustó al modelo de pseudo-segundo orden con estimación de parámetros. La luffa adsorbió 10.0 mg Cr (VI)/ g de luffa, se encontró con EDS, 1.21% de Cr en la luffa seca y 48.23% en la luffa calcinada, indicando que el Cr se encuentra en la estructura de la luffa. Con fluorescencia de rayos X (XRF) en muestra seca de luffa se tiene 8.72% de Cr y 75.07% en luffa calcinada.

Palabras clave: Cr (VI), Luffa, Cinética de Bioadsorbente, Aguas residuales.

*Corresponding author. *E-mail*: gloriam@iqcelaya.itc.mx ;
https://doi.org/10.24275/rmiq/Mat25443
ISSN:1665-2738, *issn-e*: 2395-8472

1 Introduction

A demanding issue in Guanajuato state, Mexico, is wastewater contamination with Cr (VI), primarily from the leather tanning industry associated with shoe production. This industry generates large volumes of wastewater containing significant amounts of Cr (VI). Prolonged exposure to Cr (VI) originates serious health risks, including mutagenic and carcinogenic effects (Vašková and Kolomazník, 2016). Among various methods for removing Cr (VI) from wastewater, adsorption is notable for its cost-effectiveness, particularly when using bioadsorbents made from organic or biological materials, often derived from waste. These bioadsorbents are inexpensive, easily available, and relatively easy to handle as waste management (Hasanzadeha *et al*., 2024). Some examples are the use of artichoke packed in bags as a chromium VI bioadsorbent (Rubio-Campos *et al*., 2022; Diaz-Rodriguez *et al*., 2025), biomass fungus as azo dyes adsorbent (Jiménez-González *et al*., 2024), and the use of avocado seed for the removal of textile dyes (Gonzales-Condori *et al.,* 2023).

During adsorption, atoms, ions, and molecules are retained on the surface of a material until an equilibrium is established between the dissolved solute and the solute bound to the sorbent (Khadir *et al*., 2020). This process can involve three types of interactions: physisorption, chemisorption, and electrostatic sorption (Arroyo and Cervantes, 2018). In this study, bioadsorption focuses on removing heavy metals from wastewater using biological-adsorbent sources. These materials are economically advantageous, as many are byproducts or waste materials. Their effectiveness is due to functional groups within proteins, carbohydrates, and phenolic compounds, such as carboxyl, hydroxyl, sulfate, phosphate, and amino groups (Tejada *et al*., 2018). Bioadsorbents have shown a high capacity to remove trace metals from aqueous solutions. The functional groups on their surfaces, such as hydroxyl and carboxyl, play a crucial role in binding chromium ions. Studies highlight luffa's high surface area, porosity, and eco-friendly nature, making it an efficient and sustainable option for chromium removal compared to conventional methods (Nwosu-Obieogu and Okolo, 2020, Diaz-Rodriguez *et al*., 2025).

Luffa (*Luffa cylindrica*) known as vegetable sponge gourd, is an herbaceous plant with a fibrous vascular network. It has potential as a bioadsorbent due to its lignocellulosic composition, consisting of 50-70% cellulose, 8-22% hemicellulose, and 10-23% lignin (Laidani *et al*., 2020). Luffa contains various functional groups, such as aliphatic hydroxyl, phenolic methoxyl, and carbonyl, which play a significant role in its bioadsorptive properties. These functional groups can be analyzed using Fourier-transform infrared spectroscopy (FTIR), allowing the identification of changes in the characteristic bands of the bonds associated with these groups. Such changes can indicate the occurrence of chemisorption, as they reveal chemical interactions between the Luffa functional groups and the adsorbed substances (Miretzky and Cirelli., 2010; Rahman *et al*., 2014).

The pH of the solution controls the adsorption processes of metals on different adsorbents. The adsorption of metal ions depends on the nature of the surface as well as the distribution of chemical species of the metal in the aqueous solution. The adsorption of cations favors pH values greater than 4 and the adsorption of anions at pH values ranging from 1 to 4 (Kuyucak and Volesky, 1989; Tejada-Tovar *et al*., 2018). Cr (VI) has anionic sorption behavior. Its adsorption decreases with an increasing pH, and when competing dissolved anions are present. Depending on the pH, Cr (VI) in aqueous solutions occurs in anionic form as $HCrO_4^{-1}$ or CrO_4^{-2} (Richard and Bourg, 1991; Tejada-Tovar *et al*., 2019).

The pH also affects the change in the surface area and the groups' protonation degree functionalities of the adsorbent, by having an organic material in contact with an acidic solution the functional groups are protonated, leaving the surface of the bioadsorbent with a positive charge, which favors the adsorption of $HCrO_4^{-1}$ anions which have a negative charge. It has been reported that in the range of 1-2, with increasing pH, the percentage of adsorption of Cr (VI) as an anion increases $HCrO_4^{-1}$, while in the range of 2-8, as the pH increases, the adsorption decreases, and the optimal pH was 2. It is explained that the increase in removal from pH 1 to 2 is due to the conversion of Cr (VI) species in which neutral H_2CrO_4 was formed at pH less than 2. A higher pH causes the degree of protonation of the functional groups to decrease, reducing the adsorption capacity (Sun and Hong, 2011).

When the aqueous solution of Cr (VI) has an alkaline pH, it tends to have a high concentration of -OH ions that compete with $HCrO_4^{-1}$ ions on the active sites of the sorbent's surface, drastically affecting removal.

In this study, we examined the application of luffa as a bioadsorbent for Cr (VI) removal from wastewater. Various characterization techniques were used to analyze the luffa fibers before and after the Cr (VI) adsorption process. Energy Dispersive Spectroscopy (EDS) and X-ray Fluorescence (XRF) were used to identify the elements present and corroborate the adsorption of Cr (VI). The EDS coupled with a scanning electron microscope (SEM), allowed a point analysis of the elemental composition in specific areas and at the micrometer scale. XRF

provided an average sample analysis, confirming the presence of Cr (VI) in a global technique (Komatani *et al*., 2013).

Furthermore, the morphological analysis using SEM allowed us to observe the structural and surface characteristics of the luffa fibers before and after adsorption, highlighting changes in texture and the presence of depositions attributable to Cr (VI). For its part, Fourier Transform Infrared Spectroscopy (FTIR) was used to identify the functional groups present in the fibers and evaluate the chemical interactions between the Cr (VI) species and the adsorbent surface. These coupled techniques provide a comprehensive understanding of the chemical composition and structural characteristics of Luffa fibers, strengthening the interpretation of adsorption processes.

The selection of pH in this study was based on evidence widely documented in the literature, which establishes that the optimal value for Cr (VI) adsorption using *Luffa cylindrica* and other lignocellulosic materials is approximately 2. This value is explained by the interaction between the surface properties of the adsorbent and the chemical speciation of Cr (VI) in aqueous solution. The adsorption kinetic parameters, including the adsorption equilibrium concentration of Cr (VI) on luffa (q_e) and the rate constant (k), were calculated by parameter optimization using Excel^{TM} Solver. A kinetic model was also developed to describe the adsorption of Cr (VI) on Luffa as a function of time.

2 Materials and methods

2.1 Preparation of luffa for use as a bioadsorbent

First, the luffa was washed with tap water and then dried at 90 °C for 24 hours. Subsequently, it was soaked in distilled water at 90 °C for 30 minutes and then soaked in distilled water at 25 °C for 24 hours. Later, the luffa was rinsed again with distilled water and dried to a constant weight. The luffa was cut into cubes approximately 5 mm in size to facilitate grinding and then ground using a blender to obtain luffa filaments ranging from 2 to 7 mm.

2.2 Methodology for the determination of lignin, cellulose, and hemicellulose in luffa

Nine crucibles were weighed using an analytical balance (RADWARD) and dried to a constant weight at 120 °C in an oven (Felisa, Mexico). These crucibles were then used to determine the lignin, cellulose, and hemicellulose content in the luffa samples, following the methodology outlined by Domínguez (2018).

2.2.1 Determination of lignin in luffa

A 0.2 g luffa sample was weighed, and 3 mL of 72% m/v H_2SO_4 solution was added. The mixture was stirred for 2 hours. Then 70 mL of distilled water was added. The sample was then placed in an oven (Felisa, Mexico) at 20 °C for 1 hour. Later the sample was filtered, and the residue was dried to a constant weight. The lignin percentage by weight in the luffa was determined using Equation (1).

$$\% \, Lignin = \frac{P_L \times 100}{W} \tag{1}$$

P_L weight of the lignin, g
W weight of the luffa sample, g

2.2.2 Determination of cellulose and hemicellulose in luffa

Holocellulose, which includes the combined cellulose and hemicellulose content, was first extracted from the luffa. This holocellulose was then used to determine cellulose content directly, with hemicellulose calculated indirectly by weight difference. First, 1 g of luffa (previously extracted from any other components) was weighed and placed into a 300 mL ground-glass stoppered flask. Then, 32 mL of distilled water, 0.4 g of $NaClO_2$, and 0.2 mL of CH_3COOH were added. The mixture was then heated in a Felisa oven at 70 °C for 6 hours, with an additional 0.4 g of $NaClO_2$ and 0.2 mL of CH_3COOH added every hour. After the heating, the sample was vacuum-filtered and dried at 105 °C. The holocellulose content was calculated using Equation (2).

$$\% \, Holocellulose = \frac{P_{Ho} \times 100}{W} \tag{2}$$

P_{Ho} weight of the holocellulose, g

2.2.2.1 Determination of cellulose

To determine cellulose content, 0.3 g of holocellulose was weighed, and 1.5 mL of a 17.5% NaOH solution was added to the sample. The mixture was allowed to stand for 5 minutes, followed by adding another 1.5 mL of NaOH. This process was repeated three times. Afterward, the mixture was left to stand for 30 minutes, and then 5 mL of 17.5% NaOH was added. The mixture was allowed to stand for one hour before being vacuum-filtered. The cellulose retained on the filter paper was then washed with a 17.5% NaOH solution, followed by a rinse with 100 mL of a 5% CH_3COOH solution. Finally, the cellulose was dried, and its percentage was calculated using Equation (3).

$$\% \, Cellulose = \left(\frac{P_C \times 100}{0.3}\right)\left(\frac{100}{\% \, Holocellulose}\right) \tag{3}$$

P_C weight of cellulose, g

2.2.2.2 Determination of hemicellulose

Hemicellulose content was determined by subtracting the cellulose percentage from the holocellulose percentage, as holocellulose represents the combined content of cellulose and hemicellulose. Hemicellulose was calculated using Equation (4).

$$\% \, Hemicellulose = \% \, Holocellulose - \% \, Cellulose \quad (4)$$

2.3 *Characterization of luffa*

A square luffa sample (1x1 cm) was placed under a Stemi DV4 optical microscope and observed at 32x magnification to analyze the luffa morphology. For elemental composition analysis via energy-dispersive X-ray spectroscopy (EDS), luffa filaments were mounted on a copper pin with carbon tape. Their morphology was examined using a scanning electron microscope (Thermo Fisher Phenom).

For elemental composition analysis after Cr (VI) adsorption, 2.5 g of luffa was added to 100 mL of a 500 ppm Cr (VI) solution, achieving a removal efficiency of 97.45%. Two samples were prepared: one dried at 60 °C to a constant weight and cut manually into cubes, and another calcined at 650 °C in a Thermolyne muffle furnace. The morphology and elemental composition of both samples were subsequently analyzed using SEM.

X-ray fluorescence (XRF)

The luffa beads used in the adsorption of Cr (VI) were rinsed with deionized water adjusted to a pH of 2 to remove unadsorbed residues, dried in a Felisa brand oven at 70 °C until reaching constant weight, and prepared for analysis by X-ray fluorescence (XRF) spectroscopy. For this purpose, they were uniformly distributed on a support designed to form a compact layer and ensure adequate contact with the detector in the window of the XRF equipment. An empty support was used as a blank for the initial calibration, and three measurements were taken at different points of the sample to ensure representative results. The analysis was performed via a portable XRF spectrometer Delta Prof model, configured with specific parameters for detecting heavy metals, such as chromium.

In FT-IR analysis (Thermo Fisher Scientific), luffa samples before Cr (VI) adsorption (LN) and after Cr (VI) adsorption from synthetic wastewater containing 500 ppm Cr (VI) ($LNCr^{6+}$) were placed directly on the diamond ATR crystal. Good contact was ensured by applying pressure. Twenty-five scans were performed within a wavelength range of 650 to 4000 cm^{-1}.

2.4 *Experimentation to obtain the kinetics of Cr (VI) adsorption using luffa as a bioadsorbent*

According to the NMX-AA-044-SCFI-2014 standard, used for the measurement of Cr (VI) in natural, saline, wastewater, and treated wastewater, the preparation of a stock solution, a calibration curve in the range of 0 to 1 mg/L, and the determination of Cr (VI) in the analyzed samples were carried out.

Preparation of the stock solution (500 ppm of Cr (VI))

A total of 141.4 mg of potassium dichromate $K_2Cr_2O_7$ (Karal S.A. de C.V., Leon, Gto., Mexico) with 99% purity (CAS 7778-50-9, Catalog Number K5081.0500) was weighed and previously dried at 105 °C for 2 hours. Potassium dichromate was dissolved in distilled water, and the final volume was adjusted to 100 ml in a volumetric flask.

This procedure was followed to ensure accurate measurements and compliance with the standards established by the norm. Cr (VI) 15, 20, 30, 40, and 50 ppm solutions were prepared via dilutions from a 500-ppm stock solution. The pH of each Cr (VI) solution was adjusted to 2 by adding 50 μL of a 1:1 HNO_3 solution and diluted to a final volume of 100 mL. These solutions were transferred into 125 mL Erlenmeyer flasks for batch experiments. 0.5 g of previously prepared luffa was added to each volumetric flask, following the methodology described in section 2.1. The mixtures were agitated at 210 rpm in a shaker (IKA model KS 260-C SI).

From each flask, 0.4 mL samples were taken from the initial time until 100% removal was achieved, with sampling intervals of 24 hours. Cr (VI) determination for each sample was performed in triplicate, following the NMX-AA-044-SCFI-2014 standard. A 0.1 mL aliquot from each sample was diluted with 4.9 mL of deionized water to prepare a 2:100 dilution. The pH was adjusted to 9 using 50 μL buffer solution and 30 μL of 1N NaOH solution. Then, a drop of H_3PO_4 was added to adjust the pH below 2, adding 100 μL of diphenyl carbazide. After a 10-minute development period, the absorbance of each sample was measured at 540 nm using a UV-Vis spectrophotometer (VELAB VE-5600UV), and Cr (VI) concentrations in ppm were determined from a previously established calibration curve.

2.5 *Kinetic parameters estimation for Cr (VI) adsorption using luffa as a bioadsorbent*

To perform nonlinear optimization of the kinetic model parameters for Cr (VI) adsorption, the reaction rate equation (Equation 5) was formulated, incorporating the solution volume and luffa dose, as

described in Equations (6) and (7). This setup allowed for the deduction of the adsorption rate equation (Equation 8), with Cr (VI) considered as the limiting reactive. Initial and boundary conditions were defined for each experiment at $t = 0$ ($C_t = C_i$ and $q_t = 0$) and t = t ($C_t = C_t$ and $q_t = q_t$). These conditions were substituted into Equation (9) to obtain an analytical expression for $q_{t_{est}}$, which was then compared to the experimental values $q_{t_{\exp}}$. (Sahoo and Perlot, 2020)

The method of separation of variables was applied to derive the analytical solution for estimating the Cr (VI) concentration adsorbed by the luffa *versus* time and to solve Equation (8).

$$\frac{dC_A}{dt} = kC_A{}^n \tag{5}$$

$$q_e = \frac{(C_i - C_e)V}{m} \tag{6}$$

$$q_t = \frac{(C_i - C_t)V}{m} \tag{7}$$

$$\frac{dq_t}{(q_e - q_t)^n} = kdt \tag{8}$$

$$\int_0^{q_t} \frac{dq_t}{(q_e - q_t)^n} = \int_0^t kdt \tag{9}$$

To integrate, a variable change was performed, and the initial and final conditions were evaluated (Equation 9). The yielded Equation (10) allows the estimation of the concentration of Cr (VI) adsorbed by the luffa q_t at a given time:

$$q_t = q_e - \left[kt(n-1) + (q_e)^{(1-n)}\right]^{\frac{1}{1-n}} \tag{10}$$

Where

C_A Concentration of the limiting reagent, $\frac{mg\ Cr(VI)}{L}$

C_e Equilibrium concentration, $\frac{mg\ Cr(VI)}{L}$

C_i Initial concentration, $\frac{mg\ Cr(VI)}{L}$

k Adsorption rate constant, g luffa/mg Cr (VI) h

m Luffa mass, mg

n Order of the adsorption reaction

q_e Concentration of Cr (VI) adsorbed by the luffa at equilibrium, $\frac{mg\ Cr(VI)}{g\ de\ luffa}$

q_t Concentration of Cr (VI) adsorbed by the luffa at time t, $\frac{mg\ Cr(VI)}{g\ de\ luffa}$

t Time, h

V Volume of Cr (VI) solution, L

Parameter estimation was performed using the experimental data to obtain the combined model. Given the parabolic behavior observed in the data, it was assumed that the process followed second-order kinetics, n = 2 in equation (10). Using this equation, the initial values of k and q_e were estimated for each experiment. At equilibrium, the time tends to be infinite, to find q_e, a numerical limit of 1×10^6 was used. Subsequently, the calculated values of q_e were plotted against the initial Cr (VI) concentration in solution C, showing linear behavior. Thence, the following linear model is displayed in equation (11).

$$q_e = q_0 + q_1 C \tag{11}$$

Where:

q_0 = Interception on the q_e axis.

q_1 = Slope of the line.

C = Concentration initial of Cr (VI) in the solution (mg/L).

Similarly, the estimated values of k were plotted against C and an exponential behavior was observed. This allowed the following model to be proposed, which is presented in Equation (12).

$$k = k_o e^{k_1 C^{k_2}} \tag{12}$$

Where:

k_0 = First rate constant

k_1 = Second rate constant

k_2 = Solution concentration exponent

Finally, the q_e and k models were combined and a estimation of the parameters q_0, q_1, k_0, k_1 y k_2 was performed. The parameters were optimized using Excel's Solver tool, minimizing the square error (Equation 13), allowing to determination of the optimized parameters for the estimation of q_e and k as functions dependent on the initial concentration of Cr (VI) used in synthetic wastewater.

$$E = \frac{\sum_{i=0}^{p}\left(q_{t\exp_i} - q_{t est_i}\right)^2}{p} \tag{13}$$

Where:

$q_{t_{est}}$ Estimated concentration of Cr (VI) adsorbed by the luffa at time t, $\frac{mg\ Cr(VI)}{g\ de\ luffa}$

$q_{t_{\exp}}$ Experimental concentration of Cr (VI) adsorbed by the luffa at time t, $\frac{mg\ Cr(VI)}{g\ de\ luffa}$

E Mean Square Error

p Number of experiments

3 Results and discussion

3.1 Luffa components

The analyses show that the main components of luffa, in terms of average weight percentage, are 76% cellulose, 10% hemicellulose, and 14% lignin. These values coincide with those reported in previous studies by Tanobe *et al.* (2005), Laidani *et al.* (2020), Adeyanju *et al.* (2020), and Behera *et al.* (2024), which supports the consistency of the data obtained. Furthermore, the results are contrasted with those presented in Table 1 for further comparison and validation.

Table 1. Comparison of the weight percentage of Luffa components.

Author	% Cellulose	% Hemicellulose	% Lignin
Tanobe *et al*., (2005)	63	19.4	11.2
Laidani *et al*., (2020)	60	22	10.6
Adeyanju *et al*. (2020)	57-74	1-22	0-12.8
Behera *et al*., (2024)	57-74	14-30	1-22
This work	76	10	14

Figure 1. Luffa cords under the light microscope at 32x magnification.

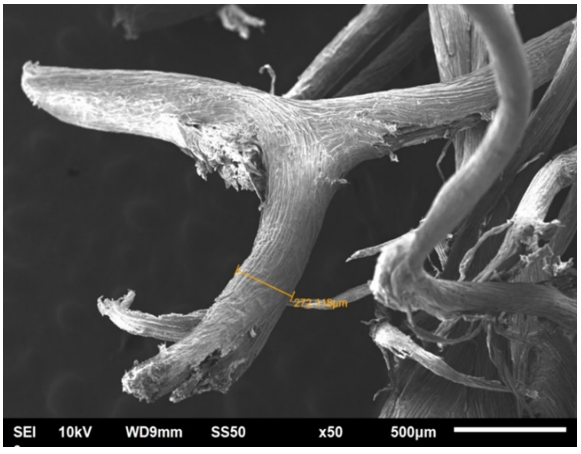

a)

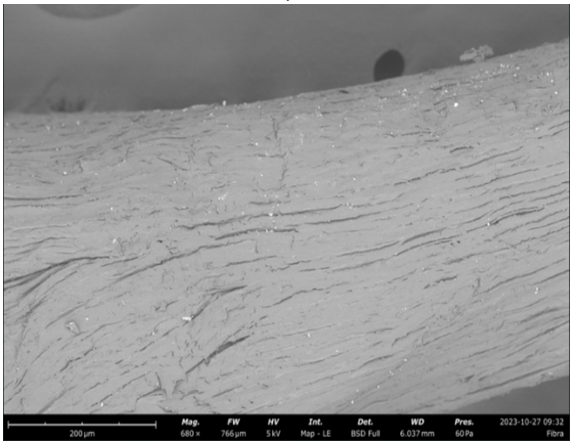

b)

Figure 2. Luffa cord observed in SEM magnification a) x50 and b) x680 (Thermo Fisher Phenom).

3.2 Luffa morphology before Cr (VI) adsorption

Optical microscopy observation at 32x magnification revealed that Luffa has a cylindrical fiber structure with irregular dimensions and rough surfaces. These fibers are interconnected, forming a network with irregular nodes, which facilitates the recovery of the bioadsorbent after the adsorption process (Figure 1).

Scanning electron microscopy (SEM) analysis provided detailed information on the Luffa bead structure, revealing fissures and diameter variations identified as potential adsorption sites for Cr (VI). A micrograph of a luffa bead is presented in Figure 2a at 50x magnification, where an average diameter of 272.119 μm is observed, along with variations in the diameters of the beads. On the other hand, Figure 2b shows the surface structure of the luffa at 680x magnification, highlighting a rough surface with fissures. This morphology is favorable for the adsorption of Cr (VI) in wastewater.

3.3 Elemental composition of luffa before Cr (VI) adsorption

Using the technique of energy dispersive X-ray spectroscopy (EDS) coupled with SEM, the main elements in luffa were determined, the results are found in Table 2. This composition highlights the predominance of organic material in the structure of luffa, which confirms its capacity as a bioadsorbent for the remotion of Cr (VI). Figure 3 shows a scanning electron microscopy (SEM) micrograph of the surface of the cylindrical luffa. The micrograph shows a fibrous structure with irregular and rough surfaces, characteristics of natural materials such as luffa, suggesting high porosity and many potential sites for adsorption. The region delimited by the box (highlighted in magenta) corresponds to the area where the EDS analysis was performed. This analysis allowed the elemental composition of the sample to be determined.

Table 2. Elemental composition of luffa before Cr (VI) adsorption.

Element	Weight %
C	49.31
O	50.69

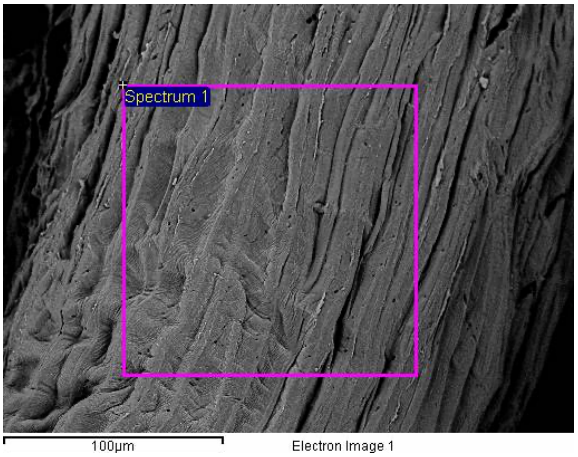

Figure 3. Micrograph for elemental composition determination of luffa.

3.4 Kinetics of Cr (VI) adsorption from wastewater using luffa as a bioadsorbent

Five experiments were conducted with initial Cr (VI) concentrations ranging from 15 to 50 ppm at a pH of 2. This acidic pH level was selected to favor the adsorption process due to the presence of $HCrO_4^{-1}$ ions, which are effectively attracted to the protonated surface of the luffa. In each experiment, 0.5 g of luffa was used as the bioadsorbent to facilitate adsorption, achieve equilibrium, and practically reach 100% Cr (VI) removal. A solution volume of 100 mL was utilized, and complete removal of Cr (VI) was achieved in all cases. The time required to reach 100% removal varied between experiments due to differences in initial concentration, with longer times observed at higher concentrations: 336 hours for 15 ppm, 432 hours for 20 ppm, 864 hours for 30 ppm, 1104 hours for 40 ppm, and 1416 hours for 50 ppm. During the initial 120 hours, a significant increase in removal efficiency was observed, with removal rates of 80%, 68%, 55%, 47%, and 45% for initial concentrations of 15, 20, 30, 40, and 50 ppm, respectively.

The parameters obtained for the equations representing the equilibrium concentration (q_e) and the adsorption rate constant (k) were determined via parameter estimation. These parameters are included in equations (14)-(15).

$$q_e = -0.29044 + 0.2437C \tag{14}$$

With MAE = 0.0261, MSE = 0.00133, RMSE = 0.03642, R^2 = 0.99986, and Error = 0.6167%

$$k = 1.46x10^9 e^{-20.904C^{0.08567}} \tag{15}$$

With MAE = 0.00003, MSE=0.00000, RMSE = 0.00003, R^2 = 0.99965, and Error = 5.6075%

$$Combined\ \ model\ for\ n = 2$$

$$q_t = q_e - \frac{1}{kt + \frac{1}{q_e}} \tag{16}$$

Where:

q_e Concentration at equilibrium of Cr (VI) adsorbed by Luffa, $\frac{mg\ Cr(VI)}{gluffa}$

k Adsorption rate constant

C Initial concentration of Cr (VI) in the solution, mg/L

These equations describe the behavior of the adsorption process and were validated through experimental data, showing their reliability for predicting both the equilibrium capacity and adsorption rate for diverse initial concentrations of Cr (VI). The equilibrium concentrations in luffa (mg Cr (VI)/g luffa) obtained from equation (15) are shown in Table 3, where it can be observed that the equilibrium concentration of Cr (VI) increases as the initial concentration increases. This indicates a good adsorption capacity of the material. However, as the initial concentration of Cr (VI) increases, the adsorption rate obtained with equation (16) decreases. This data was obtained using the pseudo-second-order model through parameter estimation.

Table 3. Optimized parameters for each initial concentration.

Removal time (h)	Legend	Initial Cr (VI) concentration (mg Cr (VI))/L	Final Cr (VI) concentration (mg Cr (VI))/L	Equilibrium concentration of Cr (VI) in luffa. (mg Cr (VI))/(g luffa)	Adsorption rate constant (g luffa)/(mg Cr (VI)*h) k×10^3
336	q_{t1}	15	0	3.365	5.196
432	q_{t2}	20	0	4.583	2.691
840	q_{t3}	30	0	7.019	1.036
1080	q_{t4}	40	0	9.455	0.515
1416	q_{t5}	50	0	11.891	0.296

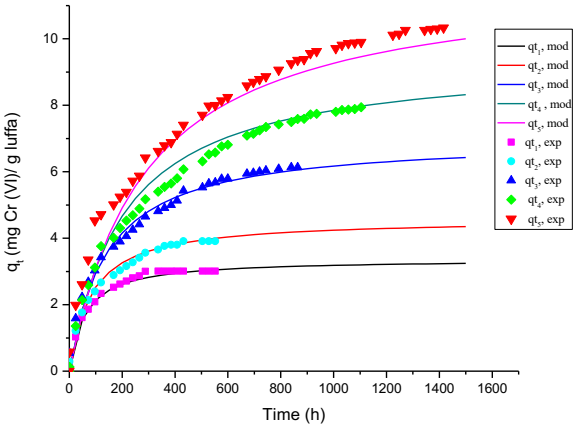

Figure 4. Predictions of combined model versus experimental values in Luffa Cr (VI) adsorption.

Figure 4 shows the evolution of the amount of Cr(VI) adsorbed per unit mass of *Luffa* (q_t, in mg Cr (VI)/g de luffa) as a function of time, for different initial concentrations of Cr(VI): q_{t1} (15 ppm), q_{t2} (20 ppm), q_{t3} (30 ppm), q_{t4} (40 ppm) y q_{t5} (50 ppm). Figure 4 depicts the experimental data (points and symbols) and the estimated values (continuous curves) obtained from the adsorption kinetics model. In general, an increase in the amount of Cr (VI) adsorbed is observed as time progresses, until an equilibrium is reached. This behavior is characteristic of adsorption processes, where, during the initial stage, the adsorption rate is fast due to the high availability of active sites on the adsorbent surface. As these sites become saturated, the adsorption rate gradually decreases until equilibrium is achieved.

The curves estimated by the model generally follow the tendency observed in the experimental data. However, small discrepancies are noted in certain time intervals, suggesting that while the model adequately describes the adsorption kinetics for the initial concentrations studied, additional adjustments may be required to improve its accuracy during the intermediate stages of the process. The results demonstrate that the adsorption capacity of Cr (VI) increases with the initial concentration and aligns well with the proposed kinetic model, validating the performance of Luffa as an effective adsorbent within the evaluated concentration range.

3.5 Luffa morphology after Cr (VI) adsorption

Figure 5a presents a 100x magnification SEM micrograph of luffa cylindrica before the Cr(VI) adsorption process. The image reveals a rough and irregular structure on the bead surface, with evident porosity details and non-uniform textures. These physical features, such as the observed roughness and porosity, are important factors that favor the adsorption capacity of the material by offering a higher

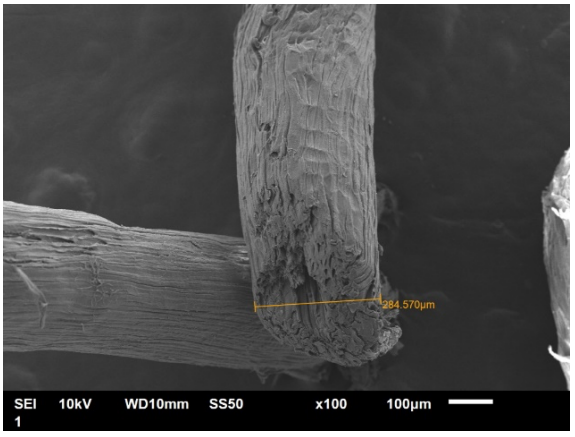

a)

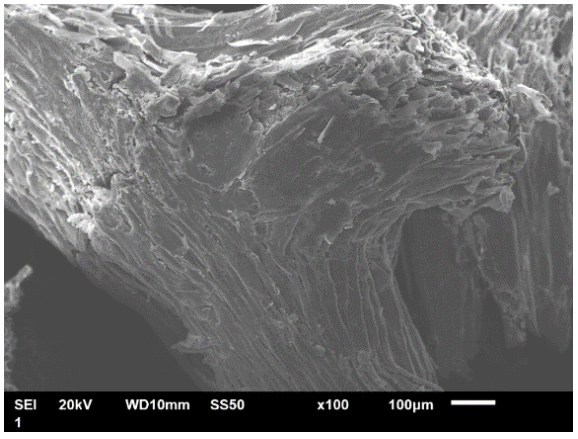

b)

Figure 5. Luffa before a) and after b) Cr(VI) adsorption observed in SEM at 100x magnification.

specific surface area and active sites available for interaction with contaminants in liquid solutions, such as Cr(VI). Figure 5b shows the SEM micrograph at 100x magnification of *Luffa cylindrica* after the Cr (VI) adsorption process. We observed that luffa fibers exhibit an irregular and rough surface, with material accumulations in certain regions. These deposits could correspond to adhered particles resulting from the adsorption, confirming that Cr (VI) was retained on the material's surface.

Figure 6 shows a SEM micrograph at 1000x magnification, providing a more detailed analysis of Luffa fibers after adsorption. In this image, particles are observed to be uniformly distributed over the surface of the fibers, along with an increase in surface irregularities. These particles can be attributed to deposits of Cr (VI) compounds, indicating that the adsorption process was concentrated in these specific regions. This finding suggests an efficient interaction between the $HCrO_4^{-1}$ chemical species in solution and the functional groups on the luffa's surface at pH = 2.

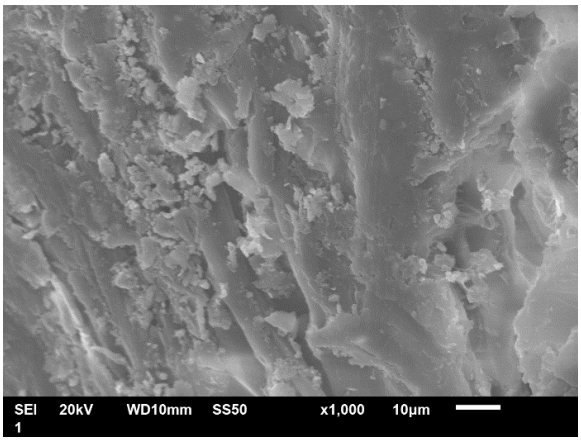

Figure 6. Luffa after Cr (VI) adsorption observed via SEM at 1000x magnification.

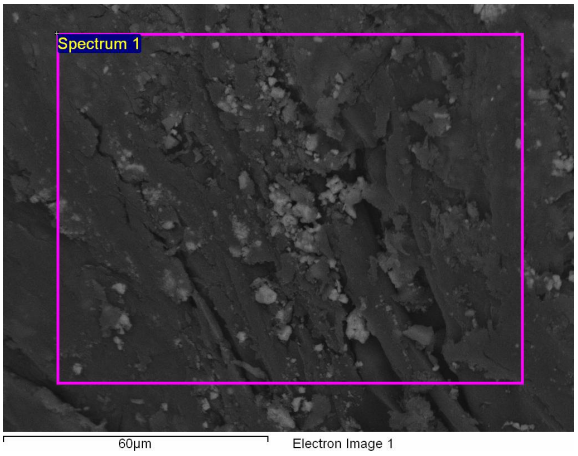

Figure 7. Micrograph for elemental composition determination of luffa after Cr (VI) adsorption.

3.6 *Elemental composition of luffa after Cr (VI) adsorption obtained with EDS*

The elemental composition of Luffa following Cr (VI) adsorption from wastewater was determined using two different procedures due to the complex structure of luffa. Luffa consists of multiple filaments with external and internal surfaces, which makes it difficult to characterize its morphology and elemental composition completely. Consequently, the analysis focused on the external surface, complemented by an examination of the luffa ash after Cr (VI) adsorption.

3.6.1 *Elemental composition of dried luffa after Cr (VI) adsorption obtained with EDS*

Figure 7 presents a micrograph obtained by SEM of the luffa after the Cr (VI) adsorption process. The image reveals a heterogeneous surface with elongated textures, where residues are randomly adhered. These residues may have originated during the adsorption process and could correspond to compounds related to the adsorbed Cr (VI) or traces of impurities.

Table 4. Elemental composition of Luffa obtained with EDS after adsorption of Cr (VI) in synthetic wastewater.

Element	Weight %
C	43.73
O	48.51
Al	0.73
Si	2.32
Cr	1.29
Fe	3.43

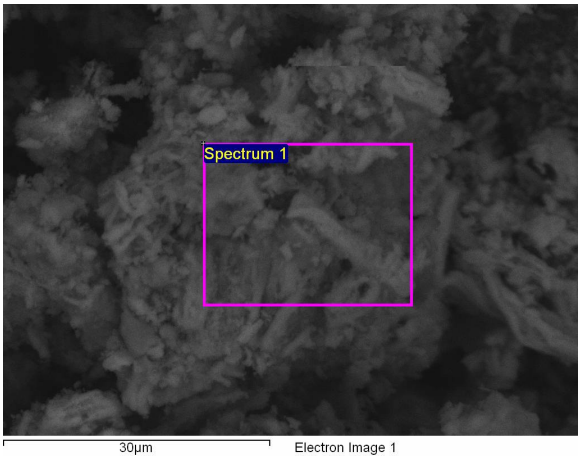

Figure 8. Micrograph for determination of the elemental composition of calcined luffa after Cr (VI) adsorption.

The elemental composition analysis was performed on the region marked as Spectrum 1.

The luffa elemental composition before adsorption consisted primarily of carbon (C) and oxygen (O). Following adsorption, additional elements were detected, including chromium (Cr) at 1.29% by weight, confirming that luffa effectively adsorbed Cr (VI) from the laboratory-prepared wastewater (Table 4).

3.7 *Elemental composition of calcined Luffa after Cr (VI) adsorption obtained with EDS*

Figure 8 depicts a micrograph obtained by SEM of the luffa calcined at 650 °C after the Cr (VI) adsorption process. The image reveals the sample morphology, featuring a porous and heterogeneous structure with particles of irregular morphology. The region for elemental analysis using EDS is highlighted via a rectangle in the image.

The elemental composition analysis of calcined Luffa after Cr (VI) adsorption revealed a Cr content of 48% weight, confirming luffa's effectiveness as a bioadsorbent for Cr (VI) from wastewater. Additionally, a decrease in oxygen (O) content and the absence of carbon (C) were observed compared

to the uncalcined sample, likely due to the thermal degradation of the bioadsorbent (Table 5).

Table 5. Elemental composition of calcined luffa after adsorption obtained with EDS.

Element	Weight %
O	41.04
Na	1.21
Si	0.65
K	8.86
Cr	48.23

Table 6. Elemental composition by XRF of dried and calcined Luffa after Cr (VI) adsorption in synthetic wastewater.

Element	Dry Luffa	Calcined Luffa
Mg	4.76	3.29
Al	0.79	1.32
Si	3.57	2.04
K	2.06	14.22
Ca	0.81	2.31
Cr	8.73	75.07
Mn	0.08	0.58
Fe	0.12	0.45
Low Energy	78.99	0.00

3.8 Elemental composition of luffa after Cr (VI) adsorption in wastewater by XRF

XRF analysis of Luffa after Cr (VI) adsorption revealed a Cr content of 8.73% by weight, along with 78.99% by weight of low-energy elements. These low-energy elements, which emit X-rays at lower energy levels, typically include light elements such as carbon (C) and oxygen (O), consistent with the organic nature of luffa. In the ash samples of luffa post-adsorption and calcination, a Cr content of 75.07% by weight was observed, with no detectable low-energy elements, attributed to the thermal degradation that occurred during calcination (Table 6).

The Cr content is significantly higher in the luffa ash after Cr (VI) adsorption from wastewater compared to the surface analysis results obtained through EDS and XRF elemental composition determination. This suggests that the entire luffa structure participates in the adsorption of Cr (VI) in the wastewater. The difference in Cr percentages between EDS and XRF is that EDS only analyzes a small region of the luffa sample, whereas XRF provides averaged elemental information over a larger volume of luffa.

FTIR spectra of luffa were obtained to understand its structure. In Figure 9 the normalized FTIR spectra of luffa fibers before adsorption (LN) and after adsorption ($LNCr^{+6}$) can be observed. The normalization criterion used was by maximum intensity (Min-Max Scaling), which scales the

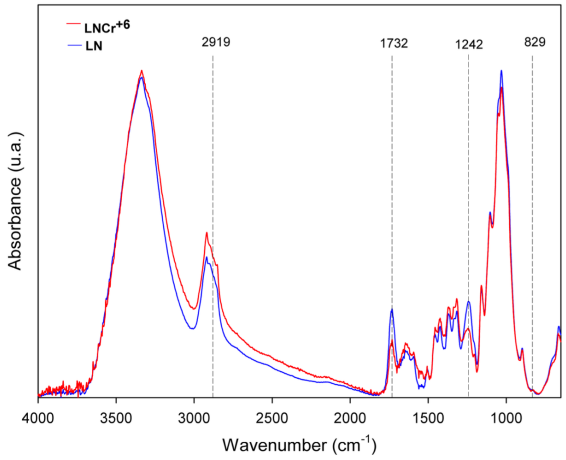

Figure 9. Normalized FTIR spectrum of luffa before and after Cr (VI) adsorption on wastewater at wavenumber 4000-450 cm^{-1}.

absorbance values between 0 and 1, A_{nom}= (A-A_{min})/(A_{max}-A_{min}). A is the original absorbance and the A_{max} value was associated with the band with the highest intensity, which in both spectra corresponded to the C-O vibration at 1030 cm^{-1} and A_{min} was assigned the value of 0 associated with the baseline of the graph.

In the LN spectrum, a broad band between ~3700 cm^{-1} and 3000 cm^{-1} (~3334 cm^{-1}), corresponds to the stretching vibration of hydroxyl groups (-OH). This functional group is present in the three molecules that make up luffa fibers. The peak at ~2919 cm^{-1} corresponds to the asymmetric stretching of CH_2 in cellulose. The sharp peak at ~1732 cm^{-1} is attributed to the C=O stretching in lignin (guaiacyl group). Peaks at ~1646 cm^{-1} and ~1506 cm^{-1} correspond to the stretching of the C=C bond in the aromatic ring of lignin. The peaks at ~1456 cm^{-1}, ~1423 cm^{-1}, and ~1370 cm^{-1} are associated to the deformation of CH_2 and CH_3 bonds (scissoring). The peak at ~1316 cm^{-1} is due to C-H bending vibrations, while the peak at 1242 cm^{-1} corresponds to C-O asymmetric stretching in the guaiacyl ring. The peak at ~1159 cm^{-1} represents C-O symmetric stretching vibrations and the peak at 1103 cm^{-1} for aromatic skeletal vibrations. Also, the peak at 1031 cm^{-1} is due to the C-O stretching in cellulose and hemicellulose, while the peak at 897 cm^{-1} corresponds to the C-O-C stretching in β-(1-4) glycosidic bonds between monosaccharides in cellulose and hemicellulose (NagarajaGanesh and Muralikannan, 2016; Vârban *et al.*, 2021).

After Cr (VI) adsorption, several differences were observed in the FTIR spectra. One of these is the peak increasing at 2919 cm^{-1}, inferring that C-H groups are involved in the adsorption of Cr (VI). Additionally, the intensities of the peaks at 1732 cm^{-1} and 1242 cm^{-1} decreased, indicating that C=O and C-O bonds are affected in the adsorption of Cr (VI). In the FTIR spectrum, no new peak was observed at 829 cm^{-1} after

the adsorption process, which typically corresponds to the Cr–O bond. This suggests that the adsorption of Cr (VI) on cylindrical luffa does not directly involve the formation of a covalent bond with chromium, but that the process may be dominated by electrostatic interactions, hydrogen bonds, or surface complexation between the functional groups present in the surface of luffa and Cr (VI) chemical species. (Perry *et al*., 1999).

3.9 Comparison of the adsorption capacity of Luffa with other materials

In this section, the results obtained for the adsorption capacity of Luffa are compared with other lignocellulosic materials reported in the literature. Table 7 describes the maximum adsorption capacities (mg/g) and the composition of cellulose, hemicellulose, and lignin for each reported material.

As can be seen in Table 7, the adsorption capacity is variable and depends on various factors such as pH, temperature, internal structure, and functional groups present in the biomaterial studied. The low adsorption capacity of Cr (VI) in *Luffa cylindrica* can be explained by its chemical composition, the nature of its functional groups, and its morphology. Luffa has a relatively low lignin content (14%), whereas other lignocellulosic materials, such as walnut hull (48.3% lignin) and coconut husk (43% lignin), have demonstrated higher adsorption capacities. Lignin contains functional groups such as phenols, carboxyls, and methoxyls, which facilitate both adsorption and Cr (VI) reduction to Cr (III), enhancing removal efficiency. Additionally, although pH 2 favors Cr (VI) adsorption in the form of $HCrO_4^{-1}$, the positive surface charge of luffa may not be sufficiently high to attract efficiently these anions. This suggests that electrostatic interaction plays a limited role in the adsorption process.

The morphology of luffa, as observed by SEM, reveals a fibrous structure with relatively large pores, which reduces the available specific surface area for adsorption compared to microporous materials. The lower density of active sites limits Cr (VI) retention on the bioadsorbent's surface. Finally, competition with other anions present in the solution may affect the material's selectivity for Cr (VI) adsorption. To improve removal efficiency, chemical modifications such as controlled oxidation or functionalization with amino and carboxyl groups, as well as physical treatments to increase porosity, could be explored. These combined factors explain the lower Cr (VI) adsorption capacity of luffa compared to other bioadsorbents and suggest that its performance can be optimized through appropriate pretreatment strategies.

Table 7. Comparison of different lignocellulosic materials on Cr (VI) adsorption and its elemental composition.

Adsorbent material	Maximum Capacity (mg/g)	% Cellulose	% Hemicellulose	% Lignin	Reference
Luffa	10	76	10	14	This work
Ground Luffa	29.98	60	22	10.6	(Laidani *et al*.,2020)
Coconut husk	29	40	0.2	43	(Tan *et al*., 1993)
Sugarcane bagasse	23	32-48	19-24	23-32	(Krishnani *et al*., 2009)
Rice husk	52.1	35	25	20	(Krishnani *et al*., 2007)
Walnut hull	98.3	33.2	9.6	48.3	(Wang *et al*., 2008)
Orange peels	16.66	13.08	6.47	6.5	(Tejeda-Tovar *et al*., 2015)
coffee waste biomass	0.827	**	**	**	(Rubio-Campos *et al*., 2022)
Activated Carbon Fiber	2.5-13	**	**	**	(Leyva-Ramos *et al*., 2008)

** Not applicable or not reported

Conclusions

This research achieved the removal of 100% Cr (VI) from laboratory-prepared wastewater using Luffa as a bioadsorbent which had an adsorption capacity of 10 mg/g luffa. The characterization of dried luffa revealed a composition of 76% cellulose, 14% lignin, and 10% hemicellulose by weight, highlighting its high cellulose content, a key component in the adsorption of contaminants. Lignin, with its carboxyl, methoxyl, and carbonyl functional groups, plays a crucial role in Cr (VI) reduction to Cr (III), which contributes significantly to the effectiveness of the material in heavy metal adsorption processes. This agrees with previous studies, such as those of Dupont and Guillon (2003), who demonstrated that, under acidic pH conditions, lignin is more effective than cellulose in the adsorption and reduction of Cr (VI). In this sense, the lignocellulosic composition of dried luffa, with a significant proportion of lignin, is decisive in its ability to adsorb and reduce Cr (VI) in aqueous solutions, since the largest amount of lignin is found in the outer surface of Luffa fibers. Scanning electron microscopy (SEM) with energy-dispersive X-ray spectroscopy (EDS) confirmed an elemental makeup primarily of carbon (56% by weight) and oxygen (38% by weight), consistent with its structural components. Fourier-transform infrared spectroscopy (FTIR) analysis identified functional groups on the luffa surface, including carbonyl, carboxyl, hydroxyl, and methoxyl groups. At a pH of 2, these groups become protonated, enhancing the chemisorption of Cr (VI) ions. Microscopy analysis revealed a rough, fissured surface structure, facilitating the physisorption of Cr (VI) onto the luffa.

An essential preparatory step involved boiling the luffa for 30 minutes, as omitting this step significantly reduced its adsorption efficiency. In experiments with synthetic wastewater containing initial Cr (VI) concentrations between 15 and 50 ppm, and using 0.5 g of luffa, complete removal of Cr (VI) was achieved. Specifically, up to 10 mg of Cr (VI) were adsorbed per gram of luffa at 50 ppm initial concentration. Adsorption time was increased with higher Cr (VI) initial concentrations, highlighting a dependence on concentration. The kinetic models indicate that Cr (VI) adsorption follows a pseudo-second-order model, with a rate constant inversely related to the initial concentration.

Finally, this study demonstrates that luffa is an effective and sustainable bioadsorbent for removing Cr (VI) from synthetic wastewater at concentrations of up to 50 ppm, achieving a 100% removal rate using 0.5 g of Luffa fibers. These findings highlight the potential for further research to assess its performance at higher concentrations, aiming to expand its application in contaminated water treatment. The findings suggest that the adsorption process involves chemisorption (as indicated by FTIR) and physisorption (as observed through SEM).

As observed in the micrographs obtained by SEM and optical microscopy, the three-dimensional structure of the luffa, formed by intertwined fibers, presents an important advantage for the recovery of the adsorbent material. Its morphology facilitates the manipulation of luffa after the adsorption process, allowing a simple separation of the aqueous medium. Additionally, the Luffa firmness prevents collapse or compaction of the fibers during the adsorption process, ensuring that the material maintains its original structure. This is especially relevant in recycling the luffa after chemical or thermal regeneration. Compared to other adsorbent materials, such as nanoparticles or fine powders, the fibrous form of luffa offers an additional advantage: it significantly reduces material loss during its recovery, making it a practical and sustainable option for water treatment applications.

These insights are the basis for future research and assessment of potential industrial applications of Luffa in wastewater treatment, contributing to the sustainable removal of heavy metals from water and addressing a significant environmental issue.

Acknowledgements

The authors thank Tecnológico Nacional de México (TecNM) for the financial support to perform the research project **"***Removal of hexavalent chromium in wastewater using luffa as a bioadsorbent*", grant 19749.24-P. We also thank CONAHCYT for the scholarship granted, which was important for finishing this work.

References

Adeyanju, C. A., Ogunniyi, S., Ighalo, J. O., Adeniyi, A. G., & Abdulkareem, S. A. (2020). A review on Luffa fibres and their polymer composites. *Journal of Materials Science*, *56*(4), 2797-2813. https://doi.org/10.1007/s10853-020-05432-6

Arroyo, I. J., & Cervantes, G. (2018). Huella hídrica de un producto industrial: una metodología (*In Spanish*). *Tecnología y Ciencias del Agua, 9*(6), 70-90. https://doi.org/10.24850/j-tyca-2018-06-03

Behera, D., Pattnaik, S. S., Mishra, P. P., Sahu, R., Manna, S., Das, N., Misra, M., Mohanty, A. K., & Behera, A. K. (2024). Fabrication

and characterization of industrial biocomposite from cellulosic fibers of *Luffa cylindrica* in a protein based natural matrix. *Industrial Crops and Products*, *212*, 118328. https://doi.org/10.1016/j.indcrop.2024.118328

Diaz-Rodríguez, K. F., Salazar-Pinto, B. M., Flores-Calla, S. S., & Gonzales-Condori, E.G. (2025). Potential use of artichoke (*Cynara cardunculus L.*) waste packed in filter bags for the removal of hexavalent chromium from water. *Revista Mexicana de Ingeniería Química, 24*(1), IA25426. https://doi.org/10.24275/rmiq/IA25426

Domínguez, J. (2018). Obtención de Materiales carbonosos y furanos a partir de bagazo de agave por carbonización hidrotérmica *(Spanish)*. Tesis de Maestría en Ciencia y Tecnología Ambiental, Centro de Investigación en Materiales Avanzados (CIMAV), Chihuahua, México.

Dupont, L., & Guillon, E. (2003). Removal of hexavalent chromium with a lignocellulosic substrate extracted from wheat bran. *Environmental Science & Technology, 37*(18), 4235–4241. https://pubs.acs.org/doi/10.1021/es0342345

Gonzales-Condori, E., Avalos-López, G., Mujica-Guzman, A., Terán-Hilares, R., Briceño, G., Quispe-Avilés, J., Parra, P., & Villanueva-Salas, J. (2023). Avocado seed powder residues as a promising bio-adsorbent for color removal from textile wastewater. Revista *Mexicana de Ingeniería Química*, *22*(3), IA2370. https://doi.org/10.24275/rmiq/IA2370

Hasanzadeha, S., Mortazavi-Derazkolab, S., & Khosravi, R. (2024). Green synthesis of iron nanoparticles using *Pistacia-atlantica* leaf extract for enhanced removal of Cr (VI) from aqueous solution. *Desalination and Water Treatment, 318*, 100347. https://doi.org/10.1016/j.dwt.2024.100347

Jiménez-González, A., Tec-Caamal, E. N., & Medina-Moreno, S. A. (2024). Biosorption performance evaluation of azo dyes Reactive Red 2 and Reactive Blue 4 on thermally sterilized biomass of *Cladosporium tenuissimum* fungus. *Revista Mexicana de Ingeniería Química*, *23*(1), IA24161. https://doi.org/10.24275/rmiq/IA24161

Khadir, A., Motamedi, M., Pakzad, E., Sillanpää, M., & Mahajan, S. (2020). The prospective utilization of Luffa fibres as a lignocellulosic bio-material for environmental remediation of aqueous media: A review. *Journal of Environmental Chemical Engineering*, *9*(1), 104691. https://doi.org/10.1016/j.jece.2020.104691

Komatani, S., Aoyama, T., Nakazawa, T., & Tsuji, K. (2013). Comparison of SEM-EDS, Micro-XRF and Confocal Micro-XRF for Electric Device Analysis. *e-Journal of Surface Science and Nanotechnology*, *11*, 133-137. https://doi.org/10.1380/ejssnt.2013.133

Krishnani, K., Meng, X., Christodoulatos, C., & Boddu, V. (2007). Biosorption mechanism of nine different heavy metals onto biomatrix from rice husk. *Journal of Hazardous Materials*, 1*53*(3), 1222-1234. https://doi.org/10.1016/j.jhazmat.2007.09.113

Krishnani, K., Meng, X., & Dupont, L. (2009). Metal ions binding onto lignocellulosic biosorbent. *Journal of Environmental Science and Health Part A*, *44*(7), 688-699. https://doi.org/10.1080/10934520902847810

Kuyucak, N., & Volesky, B. (1989). Accumulation of cobalt by marine alga. *Biotechnology and Bioengineering*, *33*(7), 809-814. https://doi.org/10.1002/bit.260330703

Laidani, Y., Henini, G., Hanini, S., & Fekaouni, A. (2020). Study of the kinetics and thermodynamics of adsorption of hexavalent chromium on the *Luffa Cylindrica* cords. *Iranian Journal of Chemistry and Chemical Engineering-International English Edition, 39*(4), 137-151. https://doi.org/10.30492/ijcce.2020.39755

Leyva-Ramos, R., Flores, J. V, Díaz, P. E., & Berber, M. S. (2008). Adsorción de cromo (VI) en solución acuosa sobre fibra de carbón activado. *Información Tecnológica*, *19*(5), 27-36. https://dx.doi.org/10.4067/S0718-07642008000500005

Miretzky, P., & Cirelli, A. F. (2010). Cr (VI) and Cr (III) removal from aqueous solution by raw and modified lignocellulosic materials: a review. *Journal of Hazardous Materials*, 1*80*(1-3), 1-19. https://doi.org/10.1016/j.jhazmat.2010.04.060

NagarajaGanesh, B., & Muralikannan, R. (2016). Extraction and characterization of lignocellulosic fibers from *Luffa cylindrica* fruit. *International Journal of Polymer Analysis and Characterization/IJPAC*, *21*(3), 259-266. https://doi.org/10.1080/1023666x.2016.1146849

Nwosu-Obieogu, K., & Okolo, B. I. (2020). Biosorption of chromium (VI) from textile wastewater using luffa cylindrica activated carbon. *Environmental Quality Management*, *29*(4), 23-31. https://doi.org/10.1002/tqem.21687

Perry, D. L., Hoi-Ying, & Dale L. (1999). Real-Time characterization of biogeochemical reduction of Cr (VI) on basalt surfaces by SR-FTIR imaging. *Geomicrobiology Journal*, *16*(4), 307-324. https://doi.org/10.1080/014904599270569

Rahman, N. N. N. A., Shahadat, M., Won, C. A., & Omar, F. M. (2014). FTIR study and bioadsorption kinetics of bioadsorbent for the analysis of metal pollutants. *RSC Advances*, *4*(102), 58156-58163. https://doi.org/10.1039/c4ra05931j

Richard, F. C., & Bourg, A. C. (1991). Aqueous Geochemistry of Chromium: a review. *Water Research, 25*(7), 807-816. https://doi.org/10.1016/0043-1354(91)90160-r

Rubio Campos, B. E., Gamiño Arroyo, Z., Murrieta Escoto, S., Méndez Segoviano, P. A., Ibarra Rivera, B. M., Jiménez Verver y Vargas, P., López Chávez, F. Y., & Álvarez Torres, X. (2022). Remoción de Cromo VI de soluciones acuosas empleando biomasa de residuos de café, *JÓVENES EN LA CIENCIA*, *16*, 1–8 https://www.jovenesenlaciencia.ugto.mx/index.php/jovenesenlaciencia/article/view/3798

Secretaría de Economía. (2014). Norma Mexicana NMX-AA-044-SCFI-2014 Análisis de agua. - medición de cromo hexavalente en aguas naturales, salinas, residuales y residuales tratadas-método de prueba (*In Spanish*). Publicado en el Diario Oficial de la Federación el 13 de enero de 2015, México. *www.gob.mx/cms/uploads/attachment/file/166148/nmx-aa-044-scfi-2014.pdf*

Sahoo, T. R., & Prelot, B. (2020) Adsorption processes for removal of contaminants from wastewater. *Nanomaterials for the detection and removal of wastewater pollutants, Chapter 7,* 161-222. https://doi.org/10.1016b978-0-12-818489-9.00007-4

Sun, M., & Hong, L. (2011). Impacts of the pendant functional groups of cellulose precursors on the generation of pore structures of activated carbons. *Carbon*, *49*(7), 2173-2180. https://doi.org/10.1016/j.carbon.2011.01.031

Tan, W., Ooi, S., & Lee, C. (1993). Removal of chromium (VI) from solution by coconut husk and palm pressed fibres. *Environmental Technology*, *14*(3), 277-282. https://doi.org/10.1080/09593339309385290

Tanobe, V. O., Sydenstricker, T. H., Munaro, M., & Amico, S. C. (2005). A comprehensive characterization of chemically treated Brazilian sponge-gourds (Luffa). *Polymer Testing*, *24*(4), 474-482. https://doi.org/10.1016/j.polymertesting.2004.12.004

Tejada-Tovar, C., Quiñones-Bolaños, E., Tejeda-Benitez, L., & Marimon-Bolivar, W. (2015). Absorción de cromo hexavalente en soluciones acuosas por cascaras de naranja (*Citrus sinensis). Rev. P+L*, *10*(1), 9-21. http://www.scielo.org.co/scielo.php?script=sci_arttext&pid=S1909-04552015000100002

Tejada-Tovar, C., González-Delgado, A., & Villabona-Ortiz, A. (2018). Adsorption kinetics of orange peel biosorbents for Cr (VI) uptake from water. *Contemporary Engineering Sciences*, *11*(24), 1185-1193. https://doi.org/10.12988/ces.2018.83105

Tejada-Tovar, C., Herrera-Barros, A., & Villabona-Ortíz, A. (2019). Assessment of chemically modified lignocellulose Waste for the Adsorption of Cr (VI). *Revista Facultad de Ingeniería*, *29*(54), e10298. https://doi.org/10.19053/01211129.v29.n54.2020.10298

Vârban, R., Crisan, I., Vârban, D., Ona, A., Olar, L., Stoie, A., & Stefan, R. (2021). Comparative FT-IR prospecting for cellulose in stems of some fiber plants: Flax, Velvet Leaf, Hemp and Jute. *Applied Science, 11* (18), 8570. https://doi.org/10.3390/app11188570

Vašková, H., & Kolomaznik, K. (2016). Spectroscopic measurement of trivalent and hexavalent chromium. *2006 17th International Carpathian Control Conference (ICCC)*, 775-778. https://doi.org/10.1109/carpathiancc.2016.7501200

Wang, X. S., Li, Z. Z., & Tao, S. R. (2008). Removal of chromium (VI) from aqueous solution using walnut hull. *Journal of Environmental Management*, *90*(2), 721-729. https://doi.org/10.1016/j.jenvman.2008.01.011